

A Low-Profile, Size-Reduced, High Gain, Circularly Polarized Anti-Jam Global Positioning System Antenna Array

Grant Evans, Jack Nemecek, Victor Obi, and Sungkyun Lim*

Department of Electrical and Computer Engineering, Georgia Southern University, Statesboro, GA 30460, USA.

ABSTRACT: A high gain, circularly polarized array antenna is proposed with low profile and compact size using T-shaped top loading, t-matching, and a reflector. Composed of 4 individual elements, the array has a -3 -dB impedance bandwidth of 1.39% (1.564–1.586 GHz) and a 3-dB axial ratio beamwidth of 79° (-42° – 37°) in measurement. The front-to-side ratio of the total realized gain pattern is 27.1 dB, and the front-to-back ratio is 25.5 dB. The peak realized gain is 11.0 dBi in the forward ($+z$) direction. The proposed antenna is a good candidate for functioning as an anti-jam antenna in global positioning system, helping to block out jamming signals coming from the horizontal (90° and 270°) planes.

1. INTRODUCTION

Global positioning systems (GPS) are commonly used for civilian and military applications, because of their ability to send real time location signals to service the user. Some of these use cases include civilian uses such as navigation and location tracking, or military uses like controlling a GPS enabled missile to hit a target with specific coordinates. GPS antennas, especially in military use, can be improved with the addition of an anti-jamming feature. Signals sent from the GPS satellite in orbit are commonly at low power levels when reaching the intended user. This is because of the long distance travelled from satellite to receiver [1]. The low power level of the signal leaves it open to directed noise, otherwise known as jamming. To help mitigate this problem, anti-jam antennas have been proposed in [2–4]. Jamming signals are generally sent from devices located on the ground. As GPS antennas are pointing in the direction of the sky (0°), any anti-jam antennas must have side radiation nulls in their 90° and 270° planes. In anti-jamming applications a thin, high gain main beam, and low gain side radiation null is preferred to nullify the amount of signal received from the ground plane. Side radiation nulls produced at the 90° and 270° planes suppress jamming signals originating from the sides of the antenna.

Typically, in GPS applications, circular polarization (CP) is needed to prevent a polarization mismatch between the satellite and users, as the satellite is at an unknown polarization when in space and orbiting the Earth. CP is used to reduce the effects of polarization mismatch as well as multipath interference. There are many different methods to generate CP; cross-dipoles, as well as different kinds of parasitic arrays have been demonstrated to generate CP [5–12]. CP is defined as having an axial ratio value below 3 dB. In [9] a method of generating CP is introduced whereby an array of antenna elements are rotated around a central axis and phase delayed by 90° . Using this tech-

nique, broadband CP is observed across the frequency range of interest. A 4-element inverted F/L antenna is proposed for GPS applications [10]. A method of using arrays with individual antenna elements rotated at different angles is shown to generate wideband CP [11, 12].

In this paper an anti-jam, 4-element GPS antenna array is proposed. The proposed antenna is low-profile, displays a high gain, and is circularly polarized within the bandwidth. The focus of this antenna is the L1 band (1.563–1.587 GHz, center frequency of 1.575 GHz) as this is one of the more common GPS frequencies. First, a study is performed on antenna size and spacing reduction between the antenna elements and a reflector. Anti-jam capabilities as well as multiple elements are then added to achieve CP. The proposed antenna is designed and simulated in Altair FEKO. A detailed overview of the proposed GPS antenna is then given. Next, the antenna array is fabricated and measured for verification of simulation results. An Agilent Technologies E5063A network analyzer is used with an anechoic chamber for measurement verification.

2. ANTENNA ARRAY DESIGN PROCEDURE

The overall design procedure is shown in Figure 1. First a standard dipole is constructed in Figure 1(a). Size reduction is needed to fit onto the reflector, so top loading [13, 14] is implemented on a dipole, shown in Figure 1(b), to reduce the overall electrical size of the antenna element. Electrical size of an antenna is typically defined by kr , where k is the wavenumber, and r is the radius of a sphere enclosing the antenna [15]. The antenna elements are designed at $0.95kr$. The S_{11} of the $0.95kr$ antenna compared to a half-wave dipole is shown in Figure 2. As shown in the figure the size reduction impact on the S_{11} of the antenna is negligible with similar bandwidth and the minimum S_{11} value.

Next, the antenna is placed over a reflector at spacing value s , shown in Figure 1(c). An analysis is performed on the effect

* Corresponding authors: Sungkyun Lim (sklim@georgiasouthern.edu).

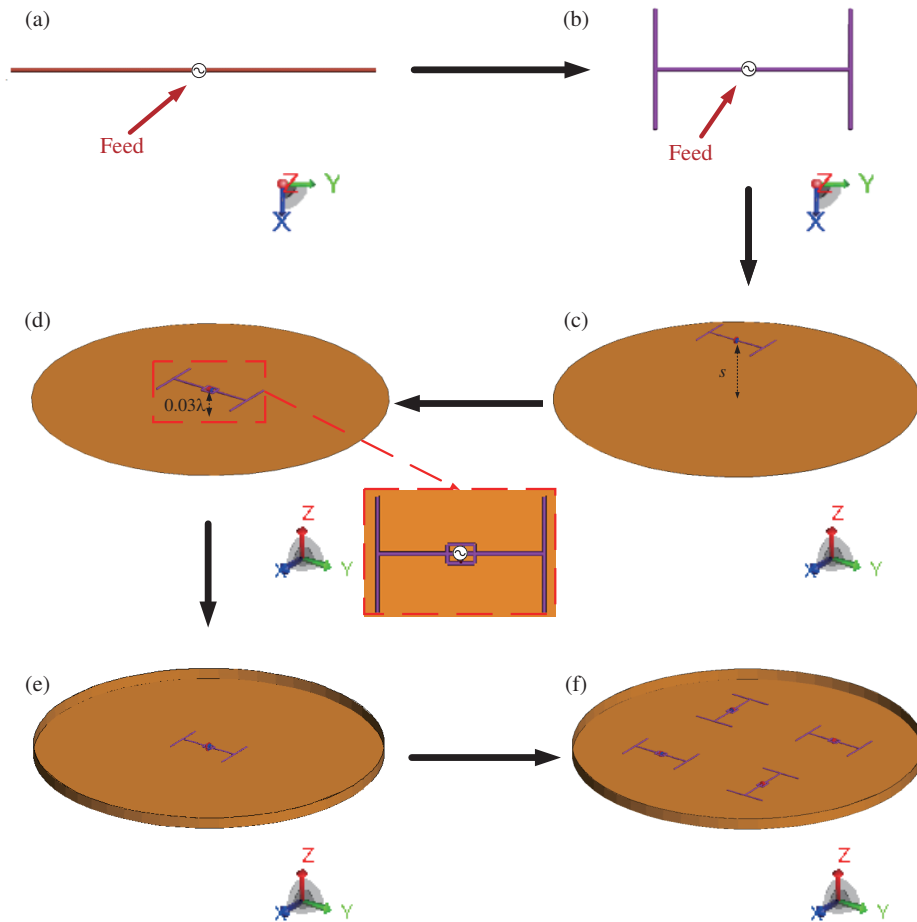


FIGURE 1. Antenna array design procedure.

of decreasing the spacing. This analysis is performed in Table 1. The spacing value s is shown from 0.25λ to 0.03λ . The values shown are the real impedance, efficiency, directivity at a theta value of 0° and 90° in the XZ plane, and the realized gain at 0° . Only the XZ plane is taken as the YZ plane contains the standard dipole null at the tips of the dipole. At 0.25λ spacing, the currents of the reflector and the radiating element are nearly in phase, leading to good impedance matching. As the spacing value is lowered to 0.03λ the currents on the radiating and reflecting element turn more out of phase, leading to poor impedance matching from the real impedance decreasing [16]. However, the directivity does not decrease but rather slightly increases as s is decreased. As directivity increases in the main beam direction, the radiation at the sides of the antenna decreases. While the 0° realized gain is shown to decrease when the spacing decreases the 0° directivity value increases by almost a full 1 dB, and the 90° decreases by nearly 2 dB when spacing is lowered to 0.03λ in comparison to 0.25λ . This is preferable for the anti-jamming application which seeks to prevent jamming from the 90° and 270° planes.

Figure 1(d) shows the next step. To obtain the gain values at the spacing of 0.03λ a boost to the radiation resistance is needed, so t-matching is added to the antenna element. The matching difference between the t-matched element and the non-t-matched element at 0.03λ spacing is shown in Figure 3.

The non-t-matched element does not function with the close spacing to the reflector mainly due to low radiation resistance, whereas the t-matched element achieves an S_{11} minimum of -14.5 dB. Figure 4 shows a front-to-side ratio comparison of each step in Figure 1. Decreasing the spacing from 0.25λ to 0.03λ increases the front-to-side ratio by 3 dB. A sidewall is added in Figure 1(e), and a small increase in front-to-side ratio is displayed in Figure 4.

Finally, 3 additional elements are added to form a 2×2 array, these elements are rotated individually as shown in [9]. Figure 1(f) presents this finalized design. Each phase is delayed by 90° , starting at the bottom most element at 0° , then going clockwise, 90° , 180° , and 270° . Adding the elements in this order with the phase shifts allows it to generate almost perfect CP over a wide bandwidth. A large increase in front-to-side ratio occurs in Figure 4 because of the addition of 3 elements. Due to the addition of these elements, the main beam is increased substantially, and the side radiation is reduced significantly.

3. DETAILED STRUCTURE OF THE PROPOSED ANTENNA ARRAY

The final proposed antenna array design and its dimensions are shown in Figure 5. Since the dimensions of the 4 elements are the same, the minimum S_{11} of all elements occurs

TABLE 1. Spacing effect of the T-top antenna over a reflector in Figure 1(c).

Spacing from Reflector (s) in λ	R_{in} (Ω)	Efficiency (%)	Directivity $\Theta = 0^\circ$ (dBi)	Directivity $\Theta = 90^\circ$ (dBi)	Realized Gain $\Theta = 0^\circ$ (dBi)
0.25	42.30	99.7	8.73	-3.73	8.69
0.20	31.90	99.5	9.10	-4.40	8.86
0.15	20.80	99.3	9.35	-4.93	8.50
0.10	10.51	98.6	9.53	-5.33	7.07
0.05	2.97	95.1	9.65	-5.57	2.68
0.03	1.15	87.5	9.66	-5.59	-1.49

Note: All values are calculated at the resonance frequency where $X_{in} = 0$.

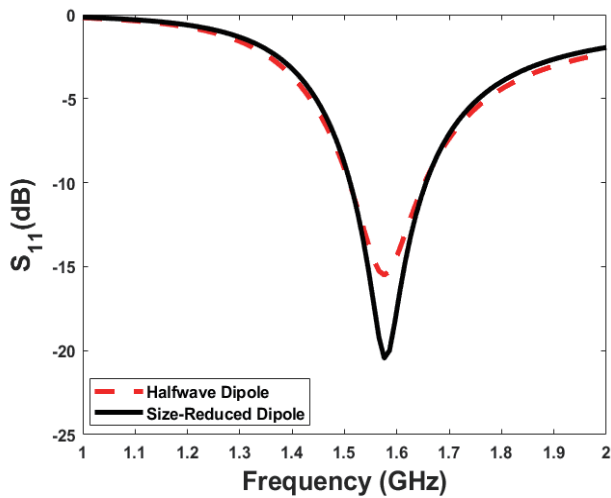


FIGURE 2. S_{11} of the antennas in free space.

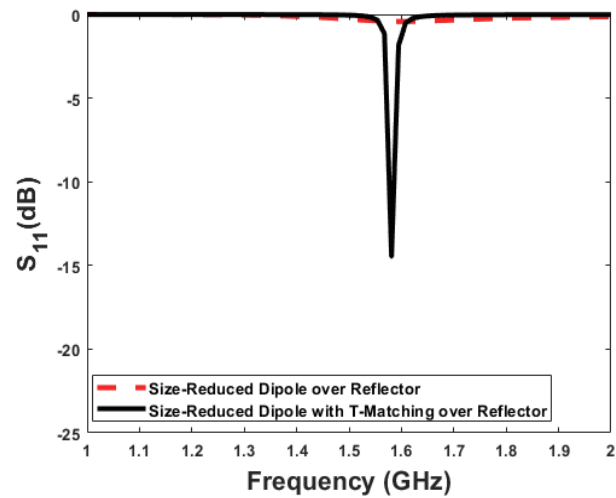


FIGURE 3. S_{11} of the antennas over a reflector spaced at 0.03λ .

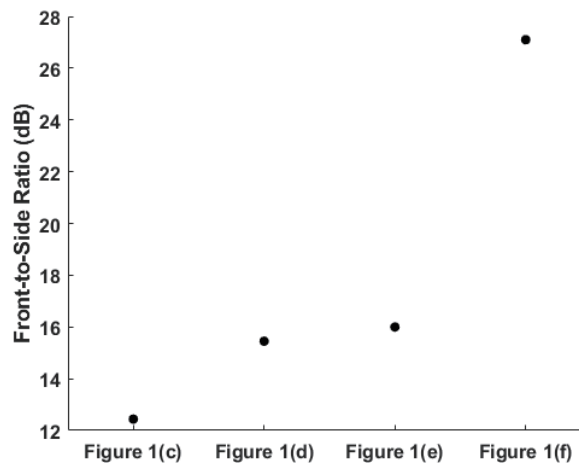


FIGURE 4. Front-to-side ratio comparison of Figure 1.

at 1.575 GHz. As the size of the reflector decreased, slight deviations in the s-parameters are noticed. The overall diameter of the reflector is to be set to a minimum radius of 0.7λ . Side wall height is noticed to affect the front-to-side ratio, whereby increasing the height of the side wall correlated with an increase

in front-to-side ratio. The overall antenna array size is intended to be low profile, so a wall height, 0.045λ , slightly higher than that of the antenna elements is used. The spacing, shown in ‘ h ’ in Figure 5, between the antenna elements and the reflector is 0.03λ . All antenna elements are the same, and the only differ-

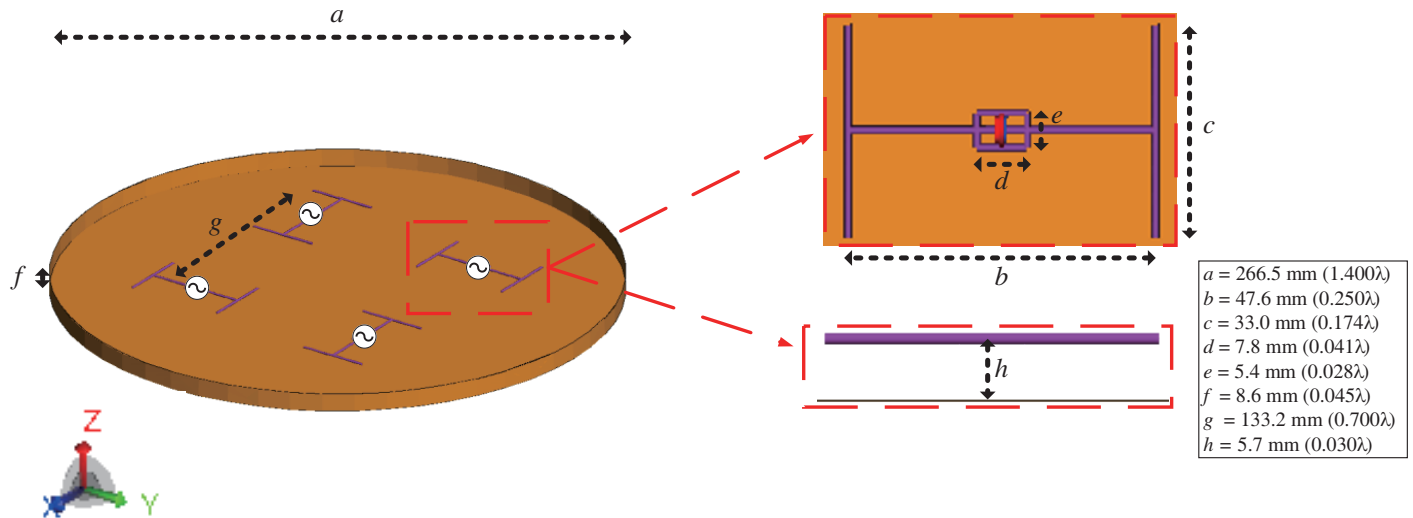


FIGURE 5. Proposed antenna array design and dimensions (λ is calculated at 1.575 GHz).

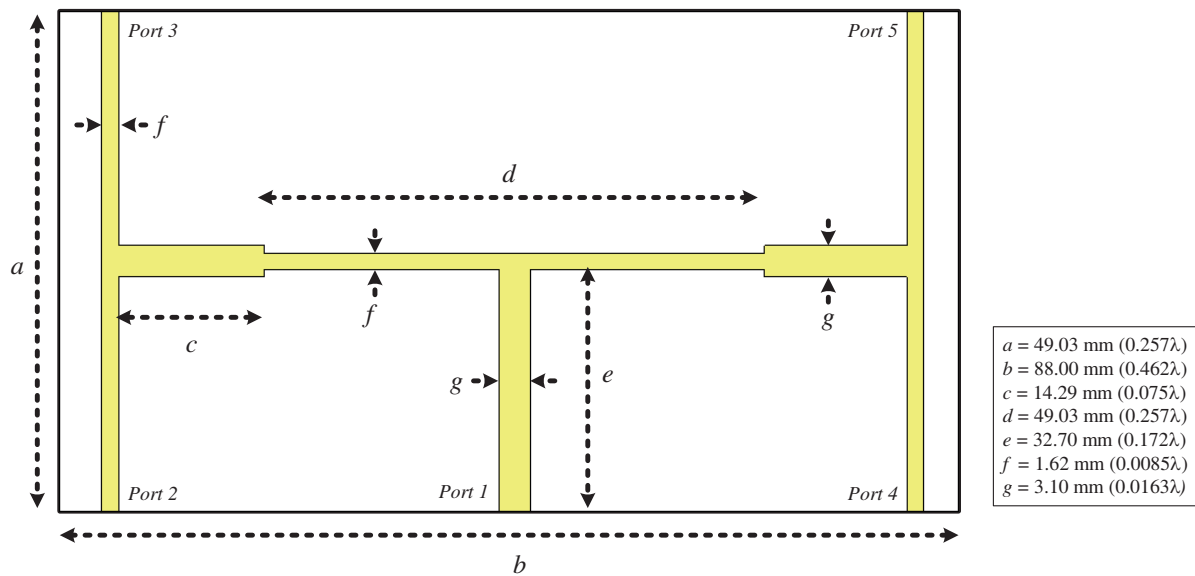


FIGURE 6. Dimensions of power divider (λ is calculated at 1.575 GHz).

ence is placement. Each antenna element is phase delayed by 90° going clockwise around the array. The phase difference in each element helps to generate CP by having 4 linearly polarized elements fed at different angles as well as phases. When put together these elements generate broadband, nearly perfect CP.

A power divider is designed in CST Microwave Studio to achieve equal power distribution across the array. The power divider is based on a quarter-wavelength transformer model whose characteristics are given in [17]. An example of a four-way split is shown in [18]. Using the basic impedances from the quarter-wavelength transformer model, the microstrip impedances were calculated [19]. The dimensions of the power divider are shown in Figure 6, where λ is calculated at 1.575 GHz. The power divider is milled from an FR-4 substrate with 1.6 mm thickness and contains a full ground plane on the

back side. The fabricated power divider is shown in Figure 7 and the simulated and measured input to output s-parameters are shown in Figure 8. The simulated vs. measurement results have good agreement. The results also match the expected value of -6 dB from input to output. In measurement some ports are favored over others due to soldering complications.

Next, prototypes of the antenna element are fabricated, shown in Figure 9. All 4 elements are the same. The feed of the array consists of 4 SMA cables connected to each of the individual elements with quarter wavelength baluns. These cables run through the reflecting element. These elements are attached to the power divider in the order specified above, rotated and phase shifted by 90° going clockwise around the array. The final fabricated design is shown in Figure 10. The individual elements are designed using 18 American wire gauge (AWG) copper wire, 0.5 mm radius. The reflector

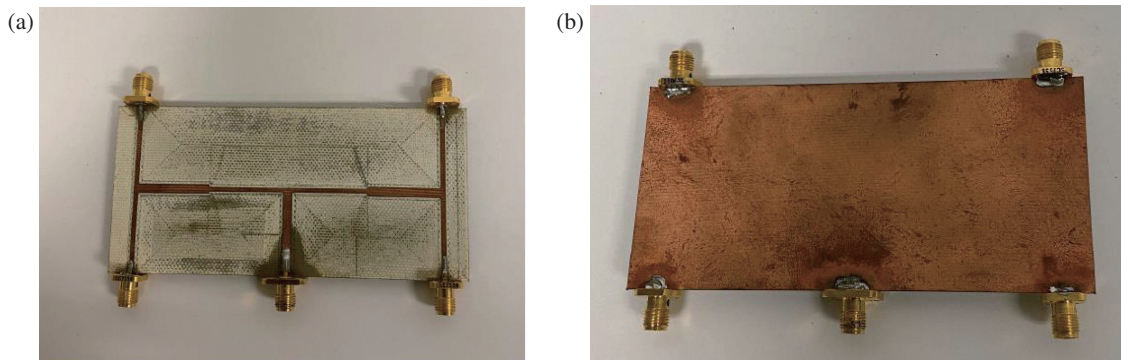


FIGURE 7. Antenna power divider. (a) Front view, (b) back view.

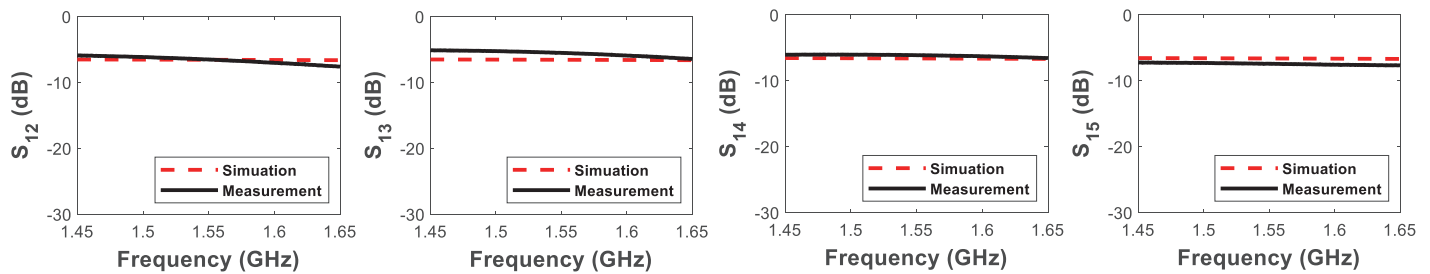


FIGURE 8. Simulation vs. measurement data for input to output S -parameters of the power divider.

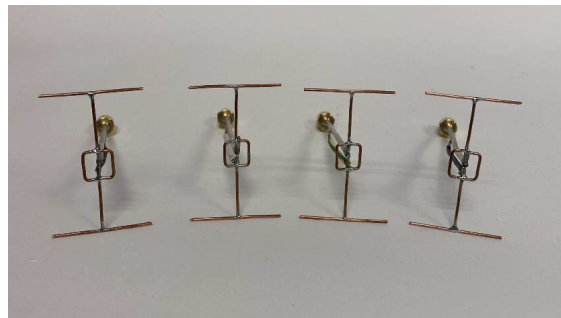


FIGURE 9. Fabricated individual antenna elements.

and wall are made of aluminum. The element spacing off the reflector is supported using balsa wood ($\epsilon_r = 1.22$) to mimic the air suspension of the antenna elements. The permittivity of balsa wood has a negligible impact on antenna measurements [20].

4. SIMULATION AND MEASURED RESULTS

The prototype antenna array is measured using an Agilent E5063 network analyzer in an anechoic chamber and compared with the simulated results. The measured S_{11} of one of the four antenna elements is shown in Figure 11. Since the design and dimensions of all 4 elements are the same, the S_{11} of only a single element of the array is depicted. As displayed in the figure the measured S_{11} closely follows the simulated trend, with the resonance occurring at 1.575 GHz. The simulated -3 -dB impedance bandwidth (IBW) is 1.14% (1.567–1.585 GHz), measured is 1.39% (1.564–1.586 GHz). The measured IBW

mostly covers the entire L1 band (1.563–1.587 GHz). In Figure 12(a) the maximum simulated realized gain in the forward ($+z$) direction is 11.0 dBi at 1.575 GHz. The measured peak realized gain in the forward direction is 11.0 dBi at 1.576 GHz and the measured realized gain at 1.575 GHz in the same direction is 10.9 dBi. In Figure 12(b) the axial ratio vs. angle plot at 1.575 GHz is shown. The simulated 3-dB axial ratio beamwidth is 66° (-33° – 33°). The measured 3-dB AR beamwidth is 79° (-42° – 37°). The array is right-handed circular polarization (RHCP) dominant in the $+z$ direction with the ability to be switched to left-handed circular polarization (LHCP) by changing the order in which the antennas are fed. The current antenna design has the antennas fed clockwise and shifting rotationally and with a phase difference of 90° each rotation. By reversing the order of the phase, performing a counterclockwise rotation instead, LHCP can also be achieved.

Next, the anti-jam functions of the antenna are analyzed by investigating the realized gain patterns at 1.575 GHz, shown in



FIGURE 10. Fabricated antenna array.

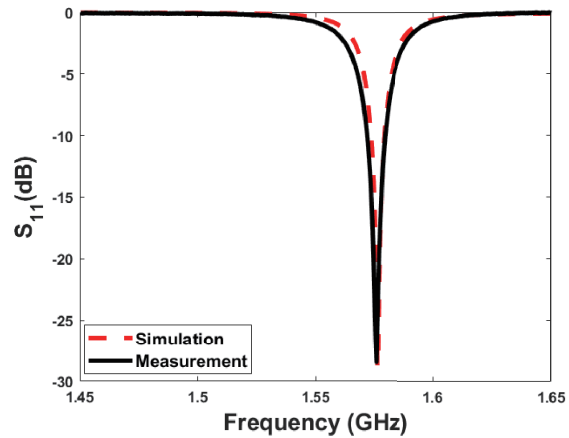


FIGURE 11. The simulated and measured S_{11} vs. frequency.

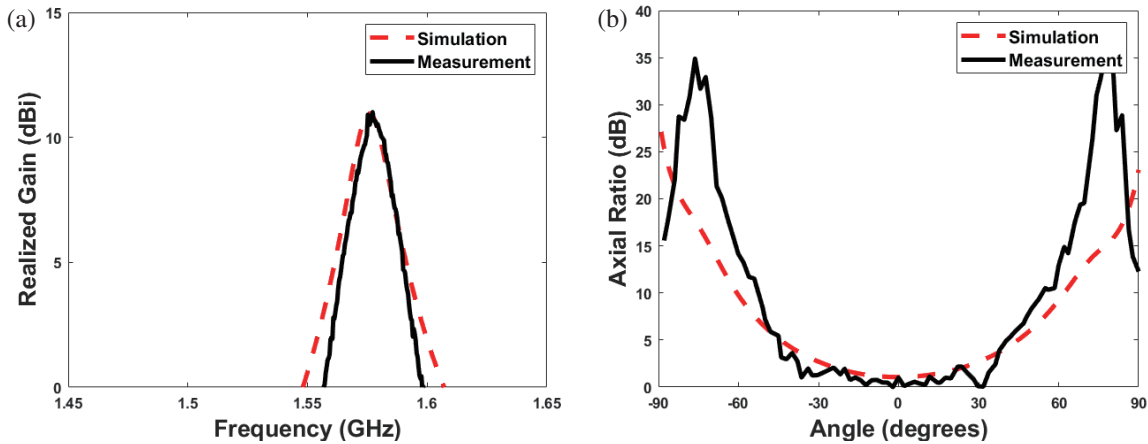


FIGURE 12. (a) The simulated and measured realized gain in the forward (+z) direction vs. frequency, and (b) axial ratio vs. angle at 1.575 GHz.

TABLE 2. Comparison to other related works.

Reference	Center Frequency, f_c (GHz)	Height (λ_c)	Peak Gain (dBi)	Circular Polarization	Mainbeam-to-Jammingnull Ratio (dB)
[2]	1.550	$0.008\lambda_c$	n/a	No	54.0
[3]	1.573*	$0.091\lambda_c$	5.0	Yes	40.0
[4]	1.575	$0.250\lambda_c$ *	8.0	No	22.5
[21]	1.575	$0.038\lambda_c$	-2.5	Yes	30.8
[22]	1.575	$0.050\lambda_c$	5.0*	Yes	20.0
[23]	1.575*	$0.530\lambda_c$	9.2	Yes	38.0
[24]	1.270	$2.168\lambda_c$ *	10.0	Yes	33.9
Proposed Antenna	1.575	$0.045\lambda_c$	11.0	Yes	27.0

Note: All values are from simulation results since some antennas do not have measurement results. λ_c is the wavelength calculated from f_c .

*Since no exact value given, result is approximated.

Figure 13. Due to the similarity of the antenna in the YZ plane, only the realized gain XZ plane is shown. The z axis being the forward-facing direction of the array. The simulated front-to-side (0° – 90°) ratio of the total realized gain pattern is 27.1 dB

and the front-to-back (0° – 180°) ratio is 26.3 dB. The measured front-to-side ratio of the total realized gain pattern is 27.1 dB and the measured front-to-back ratio is 25.5 dB. Comparing the values and patterns shows good agreement between simulated

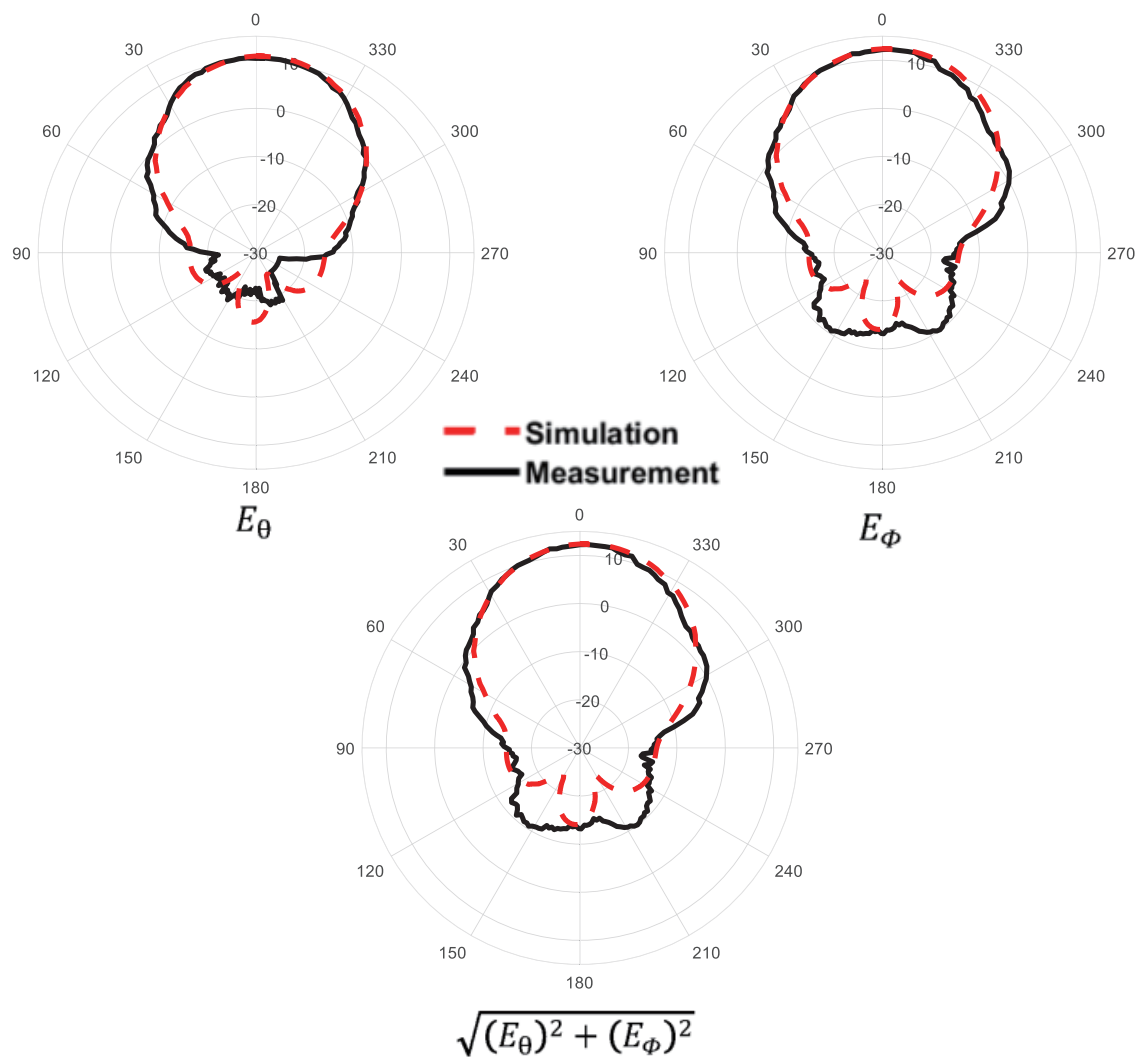


FIGURE 13. Realized gain patterns at 1.575 GHz.

and measured results. The large front-to-side ratio proves its capability to function as an anti-jam GPS antenna by heavily reducing the effect of jamming signals coming in from the horizontal (90° and 270°) plane.

Table 2 shows a comparison of values that are relevant to the proposed antenna. This includes its low-profile nature, high gain, and circular polarization. For example, in comparing height the proposed antenna displays one of the most low-profile structures with a height of $0.045\lambda_c$. The high gain is another strong point of the proposed antenna, with the highest peak gain of any observed anti-jamming antenna in this table at 11 dBi. This is while maintaining circular polarization and an acceptable jamming null in comparison to other antennas. The most comparable antenna is [24], where their peak gain is similar to the proposed antenna. While their mainbeam-to-jamming null ratio is 6.9 dB higher than the proposed antenna, the height value has been increased by a factor of 48. Another comparison would be [23], where the mainbeam-to-jamming null ratio is 11 dB higher. In this case, the height value is just over 10 times larger than the proposed antenna.

5. CONCLUSION

A low-profile, circularly polarized anti-jam GPS antenna array is proposed. First, a design procedure is shown, with the final antenna being simulated. Next, a prototype of the antenna is fabricated to verify the results found in simulation. Then, results are analyzed to see if the fabricated antenna lines up with the simulated antenna reasonably. Good agreement between simulated and measured results is shown. The measured antenna shows a -3 -dB impedance bandwidth 1.39% (1.564–1.586 GHz) and a 3-dB axial ratio beamwidth of 79° (-42° – 37°). The antenna array achieves a maximum realized gain of 11.0 dBi in the zenith direction at 1.576 GHz. The front-to-side ratio of the total realized gain pattern is 27.1 dB. Due to its high front-to-side ratio, realized gain, and CP this antenna is potentially suitable for anti-jamming GPS applications.

REFERENCES

- [1] Stutzman, W. L. and G. A. Thiele, *Antenna Theory Design*, 3rd ed., Wiley, 2013.
- [2] Zheng, Y., Y. Huang, and Y. E. Wang, "Design of small gps anti-jam antenna," in *2018 IEEE International Symposium on*

- Antennas and Propagation & USNC/URSI National Radio Science Meeting*, 1289–1290, 2018.
- [3] Rezazadeh, N. and L. Shafai, “A compact antenna for GPS anti-jamming in airborne applications,” *IEEE Access*, Vol. 7, 154 253–154 259, 2019.
- [4] Thews, J., A. O’Donnell, and J. Alan, “Design and analysis of two-dimensional parasitic liquid metal monopole array,” in *MILCOM 2017 — 2017 IEEE Military Communications Conference (MILCOM)*, 812–816, Baltimore, Md, USA, Oct. 2017.
- [5] Yu, J. and S. Lim, “Design of an electrically small, circularly polarized, parasitic array antenna for an active 433.92-MHz RFID handheld reader,” *IEEE Transactions on Antennas and Propagation*, Vol. 60, No. 5, 2549–2554, May 2012.
- [6] Lim, S., J. Chen, and C. Cato, “Design of a thin, electrically small, two-element parasitic array with circular polarization,” *IEEE Antennas and Wireless Propagation Letters*, Vol. 17, No. 6, 1006–1009, Jun. 2018.
- [7] Lu, J.-H. and C.-W. Liou, “Planar dual-band circular polarization monopole antenna for wireless local area networks,” *IEEE Antennas and Wireless Propagation Letters*, Vol. 14, 478–481, 2015.
- [8] Lin, W. and H. Wong, “Wideband circular-polarization reconfigurable antenna with L-shaped feeding probes,” *IEEE Antennas and Wireless Propagation Letters*, Vol. 16, 2114–2117, 2017.
- [9] Huang, J., “A technique for an array to generate circular-polarization with linearly polarized elements,” *IEEE Transactions on Antennas and Propagation*, Vol. 34, No. 9, 1113–1124, Sep. 1986.
- [10] Tae, H.-S., K.-S. Oh, W.-I. Son, W.-G. Lim, and J.-W. Yu, “Design of compact dual-band quadruple inverted-F/L antenna for gps 11/12 band,” *IEEE Transactions on Antennas and Propagation*, Vol. 61, No. 4, 2, 2276–2279, Apr. 2013.
- [11] Row, J.-S. and L.-K. Kuo, “Pattern-reconfigurable array based on a circularly polarized antenna with broadband operation and high front-to-back ratio,” *IEEE Transactions on Antennas and Propagation*, Vol. 68, No. 5, 4109–4113, May 2020.
- [12] Zhao, M.-Y., Y.-J. Zhu, T. Wang, T.-P. Li, B.-L. Xiao, F.-L. Niu, and X. Lei, “A wideband scanning circularly polarized array antenna based on the shorted transmission line model,” *IEEE Access*, Vol. 10, 78 493–78 501, 2022.
- [13] Chen, J., J. Ludwig, and S. Lim, “Design of a compact log-periodic dipole array using T-shaped top loadings,” *IEEE Antennas and Wireless Propagation Letters*, Vol. 16, 2017.
- [14] Yeo, J. and J.-I. Lee, “Modified series-fed two-dipole-array antenna with reduced size,” *IEEE Antennas and Wireless Propagation Letters*, Vol. 12, 214–217, 2013.
- [15] Sievenpiper, D., C. David, M. Minu, K. Tumay, K. Sanghoon, J. Long, and G. Ryan, “Experimental validation of performance limits and design guidelines for small antennas,” *IEEE Transactions on Antennas and Propagation*, Vol. 60, No. 1, 8–19, Jan. 2012.
- [16] Lim, S. and H. Ling, “Design of a closely spaced, folded yagi antenna,” *IEEE Antennas and Wireless Propagation Letters*, Vol. 5, 302–305, 2006.
- [17] Ulaby, F. T., *Fundamentals of Applied Electromagnetics*, 5th ed., Pearson Prentice Hall, 2009.
- [18] Sajjad, H., W. Tariq, K. Zeb, and A. Mairaj, “Microstrip patch antenna array at 3.8 GHz for WiMax and UAV applications,” in *2014 International Workshop on Antenna Technology: “small Antennas, Novel Em Structures and Materials, and Applications”*, month=Mar., year=2014., 107–110.
- [19] Pozar, D. M., *Microwave Engineering*, 2nd ed., John Wiley & Sons, 1998.
- [20] Smith, L., C. James, and S. Lim, “A size-reduced, 15-element, planar yagi antenna,” *IEEE Transactions on Antennas and Propagation*, Vol. 69, No. 4, 2410–2415, Apr. 2021.
- [21] Byun, G., J. Hur, S.-S. Kang, S. B. Son, and H. Choo, “Design of a coupled feed structure with cavity walls for extremely small anti-jamming arrays,” *IEEE Access*, Vol. 7, 17 279–17 286, 2019.
- [22] Awais, M., A. Madni, and W. Tanveer, “Design of a compact high isolation 4-element wideband patch antenna array for GNSS applications,” *IEEE Access*, Vol. 10, 13 780–13 786, 2022.
- [23] Hautcoeur, J. and G. Panther, “Anti-jamming GNSS antenna for timing applications,” in *2018 18th International Symposium on Antenna Technology and Applied Electromagnetics (antem 2018)*, Waterloo, Canada, Aug. 2018.
- [24] Dong, N., N. Qi, M. Guo, C. Wang, and L. Chen, “An optimal design of high gain beidou anti-jamming antenna,” in *2022 Intern. Symp. Networks, Comp. Comm.*, Shenzhen, China, 2022.